From Subsurface to Seafloor: Understanding Fault Activity Through Pockmark Mapping and Machine Learning-Driven Seismic Attribute Analysis in the NW Sicily Channel

Eshaan Sriavstava[1], Francesco Caldareri[1], Mariagiada Maiorana[1], Priyadarshi Chinmoy Kumar[2], Attilio Sulli[1]

[1]Dipartimento di Scienze della Terra e del Mare (DiSTeM) Università degli Studi di Palermo, Palermo, 90123, Italy;
[2]Seismic Interpretation Laboratory, Wadia Institute of Himalayan Geology (WIHG), Dehradun, 248001, India

Correspondence to: Eshaan Srivastava (eshaan.srivastava@unipa.it)

Abstract. This study explores fault activity and fluid migration in the NW Sicily Channel, focusing on the Adventure Plateau, using 2D seismic data, multi-attribute seismic analysis, and machine-learning-based fault detection. We assess the structural controls on fluid escape pathways and pockmark formation by applying seismic attributes such as fault probability, similarity, dip variance, and textural entropy.

Our findings reveal that pockmarks are spatially confined near structural highs, where near-vertical faults cross-cut the Terravecchia Formation and extend to the seafloor. Additionally, polygonal faults—despite hosting gas/fluids—do not contribute to pockmark formation, suggesting that tectonic discontinuities, rather than sediment compaction alone, govern active seepage.

To enhance fault characterization, we introduce a machine-learning-derived Fault Probability Section, providing a quantitative assessment of fault likelihood, surpassing traditional seismic interpretation. Our study proposes that pockmarks serve as proxies for active faulting, offering a new approach for offshore fault characterization. This method holds implications for seismic hazard assessment, hydrocarbon exploration, and geohazard monitoring.

1 Introduction

Fluid migration and seepage processes in offshore environments are key phenomena that influence seafloor morphology, subsurface fluid dynamics, and geohazards. These processes occur across a range of geodynamic settings, including rifted continental margins, subduction zones, sedimentary basins, and volcanic regions, forming fluid escape features such as mud volcanoes, carbonate mounds, gas chimneys, and pockmarks (Bünz et al., 2012; Hovland, 2012; Sun et al., 2021). The migration of fluids, particularly methane (CH_4), carbon dioxide (CO_2), and nitrogen (N_2), has significant implications for hydrocarbon prospectivity, climate change, and seafloor stability, posing potential risks to submarine infrastructure, including communication cables, offshore platforms, and pipelines(Claypool and Kaplan, 1974; Whiticar, 1999, 2002; Etiope and Milkov, 2004).

30   The Sicily Channel, situated at the boundary between the African and European plates, is a tectonically complex region shaped by a combination of compressional, extensional, and strike-slip faulting(Antonelli et al., 1988; Argnani, 1990; Civile et al., 2023; Maiorana et al., 2024) (Antonelli et al., 1988; Argnani et al., 1990, 1993; Civile et al., 2023; Maiorana et al., 2024). While much of the region has been traditionally described as an extensional domain, several studies highlight the Miocene-Pleistocene compressional deformation that has influenced the western and northwestern Sicily Channel(Volpi and al., 2022).

35   This compression has resulted in thrust systems, inversion structures, and fault reactivation, providing potential conduits for deep-seated fluid migration. Despite the tectonic complexity, studies on fluid escape features and their structural controls have primarily focused on the middle and eastern sectors of the Sicily Channel, particularly the Malta Plateau, Pantelleria Graben, and Graham Bank (Savini et al., 2009; Micallef et al., 2011; Spatola et al., 2018b, a, 2023).

In contrast, the western and northwestern Sicily Channel, including the Adventure Plateau, remains significantly understudied,
40   with limited high-resolution seismic and MBES data available to assess the interaction between faults and fluid migration pathways (Volpi et al., 2022; Civile et al., 2023). This knowledge gap is particularly critical as recent studies suggest that structural highs, including the Adventure Plateau, may host deep and shallow gas accumulations(Ferrante et al., 2022; Civile et al., 2023). However, the mechanisms facilitating fluid escape—whether active faulting, sediment compaction, or bottom current activity—remain poorly constrained.

45   Fault activity is widely recognized as a primary driver of vertical fluid migration, with seafloor depressions such as pockmarks, gas chimneys, and mud volcanoes often aligning with structural discontinuities (Spatola et al., 2018a; Ferrante et al., 2022). However, no consensus exists on the dominant mechanism governing pockmark formation in the Adventure Plateau. Some studies suggest that tectonic structures primarily control fluid migration in the region, while others propose that non-tectonic mechanisms—such as compaction, dewatering, or diffusion through sandy lenses—play a larger role (Savini et al., 2009;
50   Ferrante et al., 2022). Additionally, Maiorana et al. (2024) recently argued that pockmark distribution in the Adventure Plateau is primarily influenced by bottom currents, particularly the Adventure Bank Vortex (ABV), rather than fault activity.

This study challenges this assumption by testing whether tectonic faults exert a primary control on fluid escape in the region. Unlike previous research, we introduce a novel approach that integrates high-resolution Multibeam Echosounder (MBES) data with multi-attribute seismic analysis and machine learning-based Fault Probability Section (FPS) computation. Multi-attribute
55   seismic analysis, which has not been extensively applied in this area, enhances the detection of fault-related anomalies by integrating structural (dip variance, similarity, dip line polar) and textural (entropy, energy) attributes. FPS computation further strengthens the analysis by providing a quantitative assessment of fault activity, minimizing subjectivity in fault interpretation. By focusing on the understudied northwestern Sicily Channel, this research aims to determine whether fluid migration and pockmark formation result from active tectonism or passive non-tectonic processes. In doing so, it fills a critical knowledge
60   gap, providing a quantitative framework for offshore fault identification. The findings contribute to seismic hazard assessment, hydrocarbon exploration, and geohazard monitoring, with broader implications for active fault studies in offshore environments.

2 Study Area

2.1 Geological and tectonic setting

65 The Sicily Channel is a complex marine region, located between Sicily and Africa, with a broad and gently continental shelf, generally less than 1-2°. This geographic province includes several geological features such as ridges, volcanoes (e.g. Graham banks, Pantelleria and Linosa islands), and deep basins (e.g., Pantelleria, Malta, and Linosa grabens) (Stanley et al., 1975; Spatola et al., 2018a; Maiorana et al., 2023, 2024).

The Adventure Plateau reaches a maximum depth of about 150 meters with a shelf break at a depth of about 100 m and is
70 separated from Sicily Island by the NW–SE oriented depressions of the Mazara Channel, which connects to the Marettimo Channel and the Egadi Valley towards the north (Fig. 1).

The stratigraphy of the region is dominated by a thick Triassic–Eocene carbonate sequence (Civile et al., 2014). During the Neogene, the post-collisional convergence between the African and Eurasian plates resulted in the formation of the Sicilian Maghrebian Fold and Thrust Belt (FTB), which consists of several distinct tectonic units (Gasparo Morticelli et al., 2015; Sulli
75 et al., 2021). In the Early Pliocene, the region underwent a regional extensional event, resulting in the formation of the Malta, Linosa, and Pantelleria grabens (Fig. 1) (Catalano et al., 1993; Civile et al., 2021). Currently, the area is experiencing a mild contractional phase, particularly affecting the Malta and Linosa grabens (Civile et al., 2021; Maiorana et al., 2023). In the Plio-Pleistocene, high-angle extensional faults, primarily oriented NW–SE, have further altered the structural configuration of the area (Gasparo Morticelli et al., 2015; Parrino et al., 2022, 2023). Recent studies have also identified gas seeps and gas chimneys
80 (Fig. 2a,b) through high-resolution geophysical data, confirming the presence of active fluid flow systems throughout the Sicily Channel, including the Adventure Plateau, Graham Bank (Spatola et al., 2018b; Ferrante et al., 2022; Civile et al., 2023, Maiorana et al, 2024), and Malta Plateau (Micallef et al., 2011, 2019).

Despite this complex geological setting, the seismicity of this region is considered moderate and is mainly associated with the convergence between the European and African plates (Faccenna et al., 2004; Basili et al., 2008, 2024). Data from the INGV
85 database (ISIDe Working Group, 2007; https://emidius.mi.ingv.it/CPTI15-DBMI15/query_place/) highlights a predominant strike-slip faulting mechanism (Palano et al., 2012) (Fig. 1). Seismological studies have identified two major fault zones in Sicily, which extend offshore into the Sicily Channel. The western fault zone, trending NNE-SSW from Sciacca to Linosa Island, (Ferranti et al., 2019; Civile et al., 2021), characterized by left-lateral strike-slip faulting, volcanic activity, and elevated heat flow (Palano et al., 2020). The second fault zone is the Scicli-Ragusa Fault System, which runs from the southeastern part
90 of Sicily, from Ragusa to the offshore Sicily Channel, exhibiting a left-lateral strike-slip activity across its entire length (Catalano et al., 2008). Additionally, recent earthquake focal mechanisms in the Maltese archipelago indicate the presence of right-lateral strike-slip faults (Fig. 1) (Micallef et al., 2019).

2.2 Oceanographic Setting

In the Sicily Channel the water exchange is characterized by a two-layer model that includes the Modified Atlantic Water
95 (MAW), a relatively fresh water mass of Atlantic origin, which flows eastward into the Mediterranean, and the Levantine
Intermediate Water (LIW), a saline water mass formed in the eastern Mediterranean, which flows westward as an undercurrent
(Lafuente et al., 2002). The MAW is a shallow current, influenced by topography, coastal features, and thermohaline boundary
forces. In the Sicily Channel, it splits into two branches: the Atlantic Tunisian Current (ATC) and the Atlantic Ionian Stream
(AIS). Moreover, the MAW's path shifts seasonally with the formation of a large cyclonic eddy, known as the Adventure Bank
100 Vortex (ABV) (Robinson et al., 2001; Béranger et al., 2004). The LIW is the primary source of Mediterranean Outflow Water
and is typically confined to depths between 150 and 600 m, originates in the Ionian Sea and moves westward through the
channel south of Malta, occupying the lower part of the water column (around 250–400 m) (Incarbona et al., 2008; Gauchery
et al., 2021). Along the western edge of the Adventure Plateau, the LIW flows northwestward and, near the Egadi Islands,
turns toward the Tyrrhenian Sea (Incarbona et al., 2008; Santinelli, 2015).

105
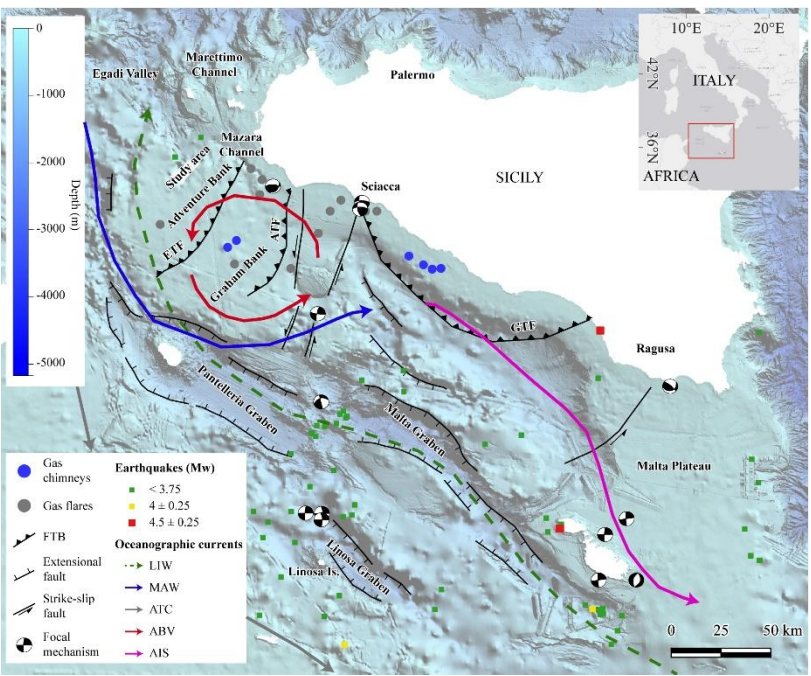
**Figure 1: Regional bathymetric map of the NW Sicily Channel highlighting the study area in white box along the Adventure Bank.
The map displays major tectonic structures, including extensional faults, strike-slip faults, and fold-and-thrust belts (FTB), along
with recorded focal mechanisms (https://terremoti.ingv.it/tdmt). Gas-related features such as gas chimneys (blue circles) and gas
flares (grey circles) are also mapped by Spatola et al., 2018a. Earthquake epicentres are colour-coded based on magnitude (Mw)**
110 **recorded between 2020 and 2025 (data from ISIDE: Italian seismological instrumental and parametric database,
http://iside.rm.ingv.it). Major oceanographic currents influencing the region are represented: LIW (Levantine Intermediate Water),
MAW (Modified Atlantic Water), ATC (Atlantic Tunisian Current), ABV (Adventure Bank Vortex), and AIS (Atlantic Ionian
Stream). The inset map shows the location of the study area within the central Mediterranean.**

3 Dataset and Software

3.1 Bathymetry information

The seafloor bathymetric data were acquired using a Teledyne SeaBat T50-P Multibeam Echosounder (MBES) system, integrated with a differential Global Positioning System for precise georeferencing. Data processing was conducted using CARIS HIPS and SIPS v.10.4, which included the removal of erroneous beams, noise filtering, calibration, navigation correction, and sound velocity adjustments to ensure data accuracy. The resulting Digital Terrain Model (DTM) was generated with a bin size of 0.5 m, providing high-resolution seafloor mapping. Interpretation of the MBES dataset (Fig. 2a) was performed using Global Mapper software (https://www.bluemarblegeo.com/global-mapper/), facilitating the identification and mapping of key seabed morphological features associated with fluid flow phenomena, such as pockmarks.

3.2 Seismic Data

Building on previous studies that employed 3D seismic data for fault and fluid migration analysis (Srivastava et al., 2017; Mandal and Srivastava, 2018; Dixit and Mandal, 2020; Kumar et al., 2021; Zhang et al., 2022), this study adopts a similar approach using 2D seismic datasets. While 3D seismic volumes provide higher spatial resolution, 2D seismic lines remain crucial for regional-scale structural interpretation, particularly in areas where 3D data coverage is limited.

The 2D high-resolution (HR) seismic dataset used in this study was acquired with a Dura-Spark sparker as the seismic source, coupled with a 48-channel digital seismic streamer (150 m long) and a 3.125 m hydrophone group interval (Fig. 2 c). The dataset has a dominant frequency of 1 kHz, providing a vertical resolution of approximately 0.4 m, making it well-suited for identifying thin beds.

The seismic interpretation was conducted using OpendTect Pro V7.0.4 (academic license) by projecting the data in a 3D environment as strike-lines and dip-lines. Additionally, seismostratigraphic analysis and 3D visualization were performed using MOVE 2022.1. Inkscape software refined and enhanced seismic imagery and structural interpretations.

135
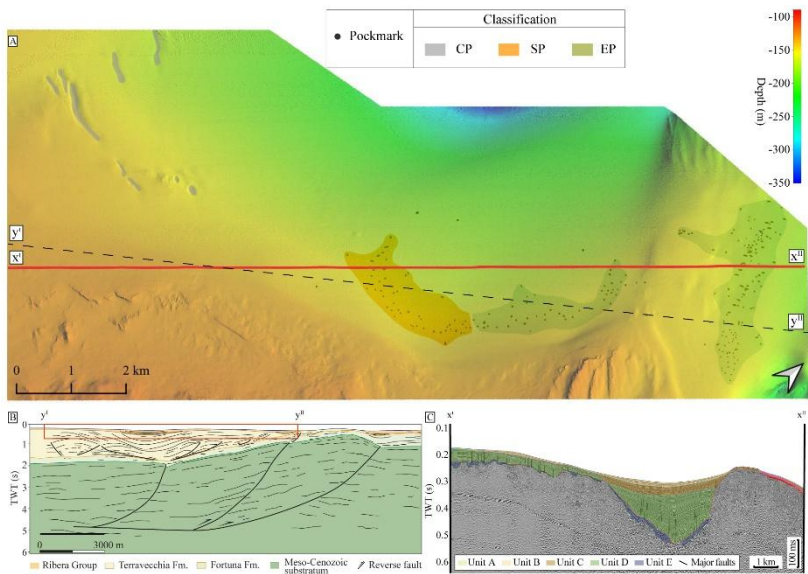
Figure 2: a) The figure shows the high-resolution DEM (3 m) of the study area with pockmark location classified as CP: Coalesced Pockmarks, SP: Sub-circular Pockmarks and EP: Elongated Pockmarks modified after Maiorana et al., 2024 along with seismic traces high resolution data (X'-X") and ViDEPI data (Y'-Y"). b) Line interpretation of the ViDEPI seismic reflection profile (Y'-Y") illustrates the study area's deep structural framework. c) It also includes the seismic section location of the high-resolution (HR)
140 **seismic profile. The seismic profile highlighted in red, whose interpretation is reported in the lower portion. Unit A: non-consolidated sediments; Unit B: group of prograding clinoforms developed from the edge of a structural high; Unit C: sheet draping external geometry; Unit D: Plio-Quaternary succession bounded at the base by a main unconformity corresponding to the top of Miocene deposits; Unit E: acoustic basement of the study area.**

4. Methodology

145 The workflow adopted in the present study is illustrated in the figure 3. To enhance the interpretability of 2D seismic data, we employed a systematic approach constituted broadly three parts: a) data conditioning, b) attribute analysis and c) neural computation.
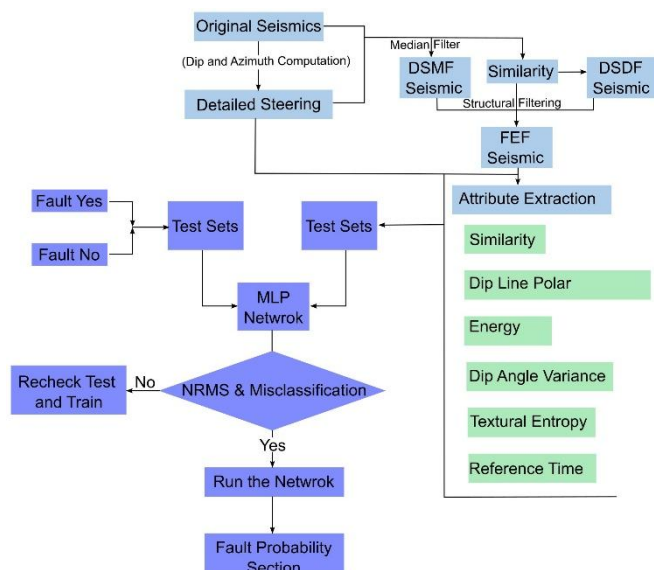
Figure 3: Workflow adopted for the present study. It consists of three parts: a) data conditioning, b) attribute analysis and c) neural computation.

4.1 Data Conditioning

The acquired 2D high-resolution (HR) seismic dataset, while providing good visibility of reflectors, remains susceptible to acoustic disturbances such as scattering, dispersion, and diffraction, which can hinder effective visualization of the subsurface architecture (Fig. 4a-c) These disturbances may partially degrade data quality, making the interpretation process more challenging and increasing the complexity of accurately mapping subsurface features (Chopra and Marfurt, 2007; Marfurt and Alves, 2014; Kumar and Mandal, 2018; Mandal and Srivastava, 2018). To overcome these challenges, the dataset was optimally conditioned to increase the signal-to-noise ratio before extracting attributes.

4.1.1 Dip-azimuth computation

The initial step in the data conditioning process involves computing dip-azimuth values to guide the application of structurally oriented filters (SOF) along the targeted seismic events (Figs. 4a-c) (Tingdahl, 1999; Tingdahl et al., 2001; Tingdahl and de Rooij, 2005). This is achieved by generating steering data for each original seismic profile using a phase gradient algorithm as the steering method, with a step-out of 1/1. The resulting high-resolution steering data serve as an input for structural conditioning, enhancing signal continuity and suppressing noise, thereby improving the clarity of seismic reflections (Figs. 4d and e).

4.1.2 Structure-oriented filters

The pre-processed seismic data still contain abrupt reflectors that degrade signal quality, as previously discussed. To address this, each 2D seismic dataset, along with its corresponding computed steering cube, is processed using a set of statistical operators designed to enhance lateral continuity and sharpen geological features imaged in the data.

The process begins with the application of a dip-steered median filter (DSMF) to smooth seismic reflections (Chopra and Marfurt, 2007a, b; Liu et al., 2009). While DSMF effectively enhances lateral continuity, it also tends to over-smooth reflectors near faults and fracture networks, potentially reducing their structural clarity. To mitigate this, an intermediate filter—dip-steered diffusion filter (DSDF) (Weickert, 1999) is applied to selectively restore fault and fracture edges by evaluating data quality within a dip-steered window and replacing central amplitude values with the most suitable estimate.

However, the DSDF can introduce noise by diffusing seismic amplitudes in regions unaffected by faults or fractures. To counterbalance this, both DSMF and DSDF are logically combined to generate a multi-attribute called fault enhancement seismic (FEF) attribute, specifically tailored for 2D seismic data. This combination integrates a pre-computed similarity attribute, where a threshold value (0.5 in this study) determines which filter is applied—DSMF is used in regions with high similarity, while DSDF is applied in areas where similarity is lower. The final output, referred to as the FEF seismic slice (Fig. 4e), enhances the sharpness of discontinuous features while reducing random noise.

The FEF seismic slice, combined with the pre-computed detailed steering cube, serves as an input for extracting reliable structural attributes, improving fault and fracture delineation for further interpretation.
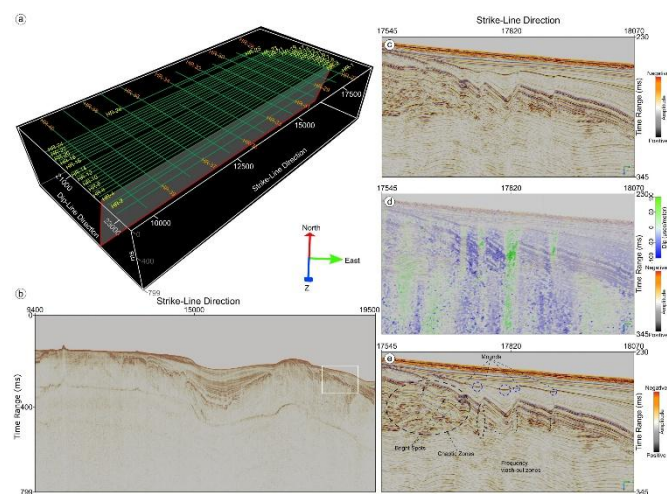
Figure 4: a) High-resolution 2D seismic dataset projected in a 3D space using OpendTect v7.0.4, comprising 26 strike-line direction profiles and 14 x-line profiles, providing spatial context for fault and fluid migration analysis. b) Original HR-3 seismic section, illustrating key structural and stratigraphic features. c) Close-up view of the HR-3 seismic section, corresponding to the white-boxed area in Fig. 4b, providing enhanced detail of reflector continuity and deformation. d) Detailed steering attribute, computed to refine reflector orientations and enhance structural interpretation, highlighting subtle discontinuities and stratigraphic trends. e) Fault Enhancement Filter (FEF) seismic section, derived from steered seismic data with applied statistical filtering, improving the signal-to-noise ratio and enhancing the visibility of bright spots, chaotic zones, frequency wash-out zones, and mounds, indicative of potential fluid migration pathways.

4.2 Attribute Extraction

The seepage of gas and fluid from stratigraphic layers is often facilitated by fault and fracture networks, leading to vertical
195 disturbances in seismic data. These disturbances typically appear as vertical zones characterized by chaotic or random textures, low amplitude, low frequency, low coherency, and low similarity. Such features manifest as shallow gas pockets, amplitude blanking (vertically oriented), direct hydrocarbon indicators (DHIs), isolated carbonate build-ups, and push-down effects within seismic slices. On the seafloor, their expressions include pockmarks and mud volcanoes (Hovland and Judd, 1988; Ligtenberg, 2003).

200 To analyze these fluid migration pathways in greater detail, this study employs a series of structural or geometric and phase attributes designed to enhance the imaging of complex geological features in seismic data.

Within the structural attribute framework, similarity, dip variance, and dip line polar were computed to identify discontinuities and fault-related structures. To enhance textural signatures, phase attributes such as energy and textural entropy were applied to each FEF seismic slice, along with the corresponding steering data.

205 Each attribute was initially defined using specific parameters, such as time gates, step-outs, and threshold values, and iteratively quality-checked across seismic lines to ensure optimal results. Once the output was deemed satisfactory, the same function was systematically applied to neighbouring 2D seismic datasets to maintain consistency and accuracy.

4.2.1 Similarity

The similarity attribute is a type of coherency measure that quantifies the degree of resemblance between two or more seismic
210 trace segments, making it an essential tool for identifying structural discontinuities, such as faults and fracture networks (Tingdahl and de Groot, 2003). It is computed by evaluating the Euclidean distance between the amplitude vectors of seismic traces along a reflection. When similarity is calculated using Fault-Enhanced Seismic (FEF) data and dip-steering as inputs, the detection of faults is further enhanced by aligning with structural dip trends (Tingdahl, 2003; Tingdahl and de Rooij, 2005). To ensure the effective identification of fault signatures across the dataset, different vertical time windows were applied
215 iteratively (Fig. 5a).

Mathematically, the dip-steered similarity between two trace segments at (xA, yA) and (xB, yB), centered at time t, is expressed as:

$$S_{dip} = 1 - \left(\frac{d_{ab}}{d_{ab}^{dip} - d_{ab}^{dip}} \right)$$

where a and b represent amplitude vectors of seismic traces within a given time window. The similarity attribute ranges from
220 0 to 1, where a value of 1 indicates identical amplitude and waveform, while a value of 0 suggests that the trace segments are phase rotated by 180°, signifying complete dissimilarity.

4.2.2 Dip Line Polar

This structural attribute helps analyses of the dip orientation and variations along seismic reflectors, making it particularly valuable for fault and fracture detection. It captures the angular variation of the dip along a defined seismic profile, allowing

225 interpreters to identify regions where structural discontinuities disrupt the dip pattern. In 2D seismic datasets, the dip line polar attribute is computed by applying dip-steering data, which aligns the seismic reflectors along their dominant structural dip and then extracts the polar representation of dip variations along the strike-line or dip-line direction. The mathematical representation of the dip line polar at a given position (x, t) is given as:

$$\theta_{dip}(x,t) = \left(\frac{dp_x}{dt}\right)$$

230 Where $\theta_{dip}(x,t)$ corresponds to the dip line polar angle at position (x, t), dp_x is the dip variation along the strike-line direction, dt is the vertical time sampling interval and lastly the inverse tangent function converts the dip rate into an angular representation.

This attribute is particularly effective in fault mapping because areas of high dip variability indicate structural discontinuities, whereas regions of low dip variability suggest uniform stratigraphic layers.

235 ### 4.2.3 Dip Variance

Dip variance is a statistical measure that effectively highlights abrupt changes in reflector dip, proving invaluable for structural interpretation, particularly in faulted regions. In 2D seismic data, where information is inherently constrained to a single plane, dip variance is computed along a single direction. This calculation utilizes dip line polar attributes and corresponding steering data, with variance serving as the output statistic. To optimize results, an iterative approach is employed, varying time gates

240 from 0.2 to 1 ms with a 1 ms step. This statistical analysis of seismic data provides crucial insights into lateral dip variations, facilitating the identification of potential fault planes and potential fluid migration pathways (Tingdahl, 2003; Tingdahl and de Rooij, 2005).

For a 2D seismic profile, dip variance in the x-direction (strike-line direction) can be mathematically expressed as:

$$var(\rho_x) = \frac{1}{n-1} \sum_{t_1}^{t_2} px(x, t+\tau) - \underline{\rho_x})2$$

245 Where t_1 and t_2 represent the relative start and stop times of the window, n is the total number of samples within the defined time window, p_x represents the dip in the strike-line direction, and $\underline{\rho_x}$ is the mean dip within the time window.

Due to the inherent limitations of 2D seismic data, lacking the dip-line (y-direction) component present in 3D datasets, dip variance calculations are restricted to variations along either the strike-line or dip-line directions. Despite this limitation, this 1D statistical approach provides a robust means to delineate faults and fracture zones, where abrupt dip variations serve as

250 strong indicators of structural discontinuities (Fig. 5b).

4.2.4 Energy

The energy attribute quantifies amplitude variations within a seismic slice, making it a valuable tool for identifying structural discontinuities such as faults and fractures. It is mathematically defined as the sum of the squared amplitudes within a specified time window (Tingdahl, 2003), expressed as:

255

$$E = \sum_{\tau=t_1}^{t_2} u(x, y, t + \tau)^2$$

where t_1 and t_2 represent the relative start and stop times of the analysis window, which are iteratively adjusted to ensure optimal results.

Regions associated with faults and fractures typically exhibit low-amplitude and low-energy anomalies, as seismic waves experience scattering, absorption, or diffraction due to structural discontinuities (Fig. 5c). Thus, the energy attribute enhances
260   the visibility of faulted zones by differentiating them from surrounding intact reflectors.

4.2.5 Textural Entropy

The textural entropy attribute is a seismic texture analysis tool that quantifies the level of disorder or randomness within a seismic dataset. Derived from gray-level co-occurrence matrix (GLCM) analysis, this attribute highlights areas with high heterogeneity, making it particularly effective for detecting faults, fractures, and chaotic geological features.
265   Mathematically, textural entropy (TE) is computed as:

$$TE = \sum_i p_i \, log \, p_i$$

where p_i represents the probability of occurrence of a particular gray-level intensity within a defined window.

In this study, textural entropy was extracted using FEF slices, with steering data as an input, ensuring optimal structural alignment before applying texture analysis. A varying time gate ranging from 0.3 to 2 ms was used to capture the vertical
270   variability in seismic textures, while a GLCM window size of 16×16 was selected to balance resolution and computational efficiency.

Since faults and fractures introduce abrupt changes in seismic texture, regions with high textural entropy correspond to structurally complex areas, whereas low-entropy zones indicate stratigraphically continuous regions (Figs. 5d and 6).
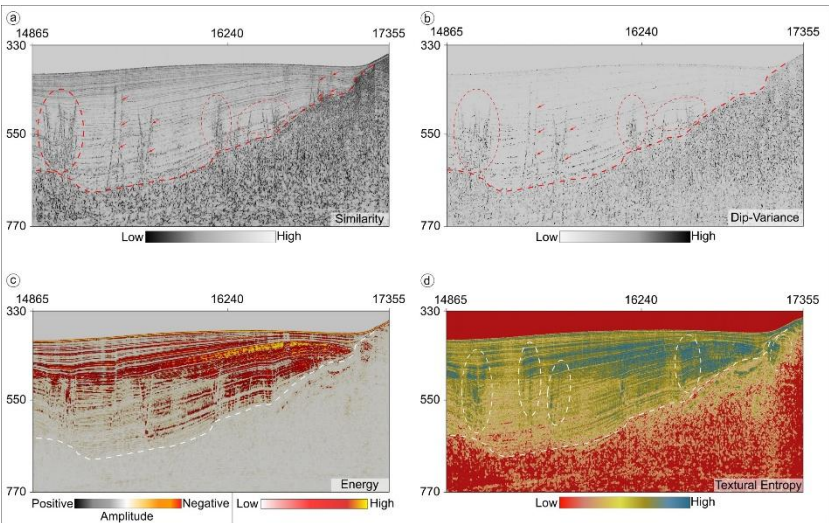
Figure 5: Seismic attribute analysis highlighting structural discontinuities and potential fluid migration pathways. (a) Similarity attribute, emphasizing lateral reflector coherence. Low similarity values (darker zones) indicate distorted or discontinuous reflectors, correlating with faulted regions and vertical fluid escape structures (red dashed circles). (b) Dip-variance attribute, accentuating lateral dip variations. High dip-variance values mark areas of deformation, aligning with fault zones and potential migration pathways. (c) Energy attribute, illustrating reflectivity strength. Low-energy zones indicate disrupted reflectors, while high-energy regions highlight intact stratigraphy and structural interfaces. (d) Textural entropy attribute, providing insights into seismic facies variability. High textural entropy values (blue-yellow zones) correspond to chaotic, heterogeneous areas, commonly associated with fluid migration and fault intersections, whereas low values (red zones) indicate more homogeneous sedimentary layers.
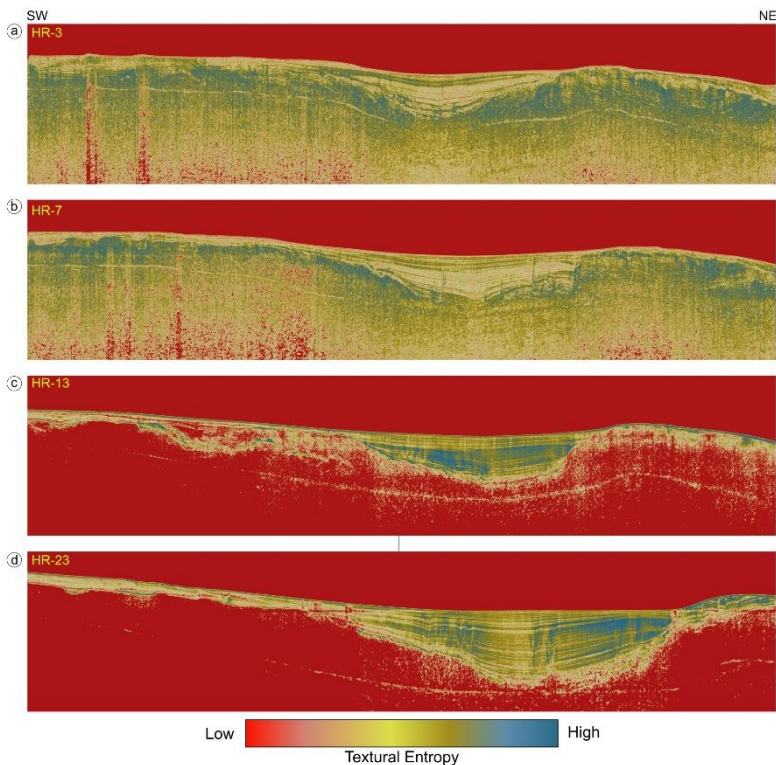
Figure 6: Textural entropy attribute analysis across multiple seismic sections (HR-3, HR-7, HR-13, and HR-23) illustrates
variations in subsurface heterogeneity and potential fluid migration pathways. High textural entropy values (blue-yellow
zones) indicate chaotic, heterogeneous reflectors associated with faulted and fractured zones, suggesting active fluid movement
and structural deformation. In contrast, low textural entropy values (red zones) may be inferred as well-stratified, homogeneous
sedimentary layers with minimal disruption. A progressive decrease in chaotic zones from HR-3 to HR-23, particularly away
from the structural high, suggests a reduction in fluid migration intensity, reinforcing the hypothesis that fault-controlled
seepage is more concentrated near structural highs, while more distal regions exhibit reduced fluid influence.

4.3 Neural Network

4.3.1 2D Seismic Dataset Adoption

Following the extraction of seismic attributes from each 2D seismic slice, a meta-attribute known as the Fault Probability
Section (FPS) is generated. This is achieved by integrating multiple extracted attributes through a Multi-Layer Perceptron
(MLP) neural network (NN), which consists of three layers: an input layer, a hidden layer, and an output layer. The MLP is a
supervised classification method, meaning it requires user-provided training examples to learn the relationship between seismic
attributes and fault probability (Ligtenberg, 2003; Jahani and Mohammadi, 2019; Veheddoost et al., 2020). Due to its iterative
learning mechanism, MLP is also referred to as a back-propagation network, as it continuously adjusts its weights to minimize
the difference between predicted and actual outputs (LeCun, 1985; Rumelhart et al., 1986; Hashemi et al., 2008; Singh et al.,
2016).

The MLP model operates based on two fundamental principles: abstraction and generalization (Fahlman, 1988; Brouwer et
al., 2011; Singh et al., 2016). Abstraction allows the network to extract relevant features from seismic attributes while
discarding noise and irrelevant variations. Generalization ensures that the trained model can predict fault probability for unseen
seismic data by establishing a mathematical relationship between input attributes and output fault probability values.

The back-propagation learning mechanism iteratively adjusts the model's weights by minimizing the error between predicted
and actual outputs through random weight initialization. The weighted sum (W) of the input features is computed as follows
(Brouwer et al., 2011):

$$W(y) = \sum_{n=0}^{L} W_n \, y_n$$

where y represents the input vector, W denotes the weights, and n ranges from 0 to L (the total number of inputs). The computed
weighted sum is then passed through an activation function (A) to produce the meta-attribute:

$$A(W) = \frac{2}{1 + exp(-W)} - 1$$

The activation function used in this study is a non-linear sigmoid function, which outputs values between 0 and 1, forming a binary classification for fault detection. In this case, output values are classified as (1,0) or (0,1), corresponding to fault-present and fault-absent regions, respectively (Tingdahl et al., 2001).

315 For training the NN, 60–70% of the training locations were used, while the remaining 30–40% were reserved for validation for each seismic slice (Fig 7a). After successful training, the trained NN model was applied to the entire 2D seismic dataset to generate the FPS. This section represents a probability volume with values ranging approximately between 0 and 1, where: Low probability values (~0) indicate regions with continuous reflectors, suggesting fault-absent areas where as high probability values (~1) confirm the presence of abrupt reflector discontinuities, indicative of faulted zones (Fig. 7b).

320 The performance of the trained NN model is evaluated using two unbiased statistical measures: normalized root mean square (nRMS) error and misclassification percentage (Fig. 7c) (Tingdahl et al., 2001). The nRMS error quantifies the deviation between the training dataset (selected by interpreters) and the test dataset (predicted by the neural network) on a scale of 0–1, while misclassification percentage represents the percentage of mismatch between these two datasets (Fig. 7d). These validation metrics ensure the reliability of the FPS in detecting fault-related discontinuities in 2D seismic data.
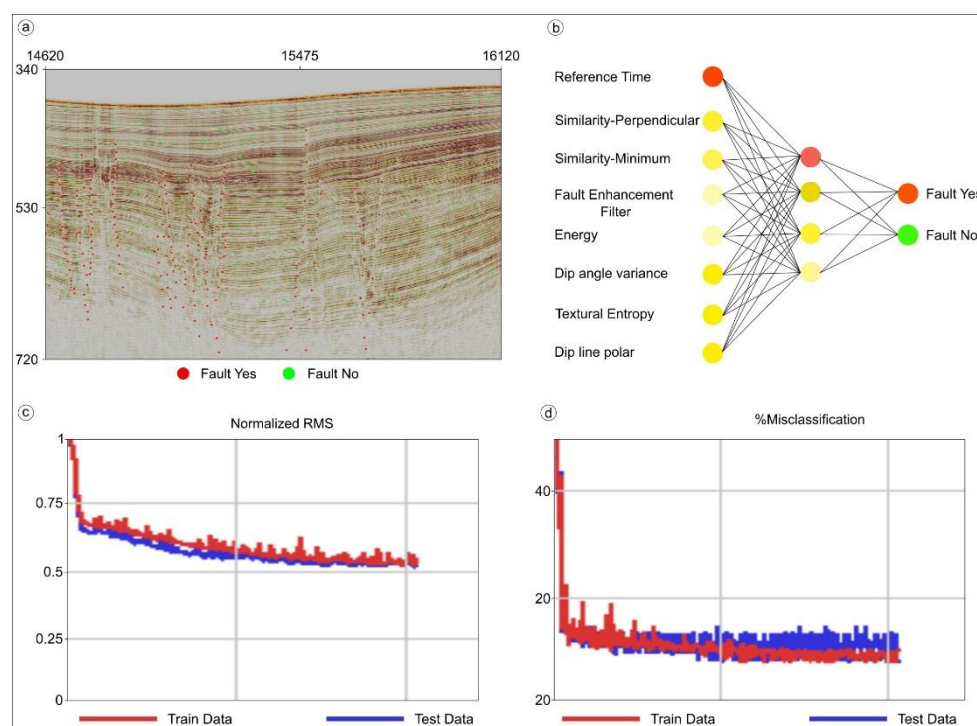
325

Figure 7: Neural network-based fault classification applied to the 2D seismic dataset. (a) Fault probability map overlaid on the seismic section, where red points indicate predicted fault locations and green points represent areas classified as non-faulted zones. (b) Neural network architecture used for fault prediction, incorporating seismic attributes such as similarity, fault enhancement filter, energy, dip angle variance, and textural entropy. (c) Normalized root mean square (nRMS) error

330 convergence plot showing model training progression, with both training (red) and test (blue) data stabilizing between 0.5 and

0.75. (d) Misclassification rate plot, indicating a decrease in error during model training, with final values stabilizing around 20–25%. The results validate the neural network's ability to detect faults, although some uncertainties persist due to attribute limitations and the absence of dip-line data.

4.3.2 Limitations

335   The application of NNs for fault probability estimation in 2D seismic data presents several limitations compared to 3D seismic analysis. A key constraint is the lack of dip-line information, as 2D seismic profiles capture structural details along a single plane, restricting the NN's ability to accurately detect fault terminations and subtle discontinuities. This results in higher normalized root mean square (nRMS) error and misclassification rates compared to 3D seismic-based models, as observed in this study (Fig. 7c, d). Additionally, reduced attribute sensitivity in 2D seismic data hinders fault detection, as attributes such

340   as dip variance and steered similarity are confined to a single dimension, whereas 3D seismic data benefits from multi-azimuth analysis.

Furthermore, sparse training data in 2D seismic limits the NN's ability to generalize fault patterns, increasing the risk of overfitting. Seismic noise and processing artifacts can also be misclassified as faults, leading to higher false-positive rates. Lastly, trained models lack transferability across different geological settings, requiring extensive retraining. Despite these

345   challenges, NN-based fault detection was systematically implemented in this study, with over 100 iterations per seismic slice, allowing for an optimized interpretation that minimized nRMS error and misclassification values.

5. Results

The seismic attribute approach, incorporating both geometric and textural attributes, has successfully delineated detailed fault and fracture zone signatures in the NW Sicily Channel. This process involved a step-wise workflow, from data conditioning

350   to multi-attribute analysis. Each attribute enhances the visualization of continuous and discontinuous reflectors, which are then integrated into a neural network to identify fault and fracture-prone zones across the 2D seismic dataset.

5.1 Fault Network Characterisation

The extracted attributes and multi-attribute analyses, incorporating FEF seismic data and detailed steering as inputs with varying time windows and step-outs, provided a comprehensive examination of reflector characteristics, including frequency,

355   phase, and amplitude. The similarity attribute, co-rendered with amplitude, highlights distorted reflectors as regions of low similarity values (Fig. 5a). These low-similarity zones effectively delineate near-vertical faults, ranging between 190 and 450 ms on both ends of the 2D seismic dataset. These vertical faults, which cross-cut the section, are more pronounced near the structural high, particularly between HR-1 and HR-9 seismic slices. In contrast, the basinal region exhibits more randomly distributed distorted reflectors with no clear directional trends. However, as the mid-basinal part thickens from HR-1 to HR-

360   26, these discontinuous structures, classified as polygonal faults, become more prominent and increase in density, with depths ranging approximately from 230 to 550 ms (Figs. 2b, 4b, 5a, 8).

Similarly, the dip variance attribute, derived from dip line polar and detailed steering data, enhances the visualization of structural complexity by highlighting lateral dip variations within the seismic dataset. Higher dip variance values correlate with faulted zones, confirming deformation along structural discontinuities (Fig. 5b). The attribute successfully delineates

365   vertical faults, with pronounced variance observed near the structural high, particularly between HR-1 and HR-9. Within the basinal region, polygonal faults exhibit distinct dip variations, with their presence becoming more pronounced from HR-1 to HR-26. These faults are capped by recent Quaternary sediments, restricting their vertical extent.

The textural attributes, energy and textural entropy, further validate the identification of faults, fractures, and potential fluid migration pathways. The energy attribute reveals low energy values in discontinuous zones, indicating disrupted reflectors

370   associated with faulted regions. In contrast, textural entropy exhibits high values in these same zones, reinforcing the likelihood of fluid migration. Notably, textural entropy peaks near the structural high, showing high values from HR-1 to HR-11, suggesting that these faults and fractures are active migration conduits (Fig. 5c and 5d). However, as one moves further into the deeper basinal region, textural entropy decreases significantly, implying a reduction in active fluid migration on the either side of the structural highs but the shallow gas emissions are evident in the basinal section were polygonal   faults are

375   getting dense with each seismic slice towards the NW i.e., HR-1 to HR-26 (Fig. 6).

5.2 Neural Computation Aiding Interpretation

A meta-attribute FPS was computed using extracted seismic attributes through machine learning approaches, providing an additional layer of confidence in fault and fracture mapping within the study area. While the neural network computation was performed on individual seismic slices, FPS offers a quantifiable metric that enhances interpretation derived from normalized

380   RMS (nRMS) and misclassification rates of both train and test datasets, which approximately ranges from 0.5 to 0.75 and 20-25%, respectively. These values indicate that while the model effectively captures fault patterns, some residual errors persist due to complex fault geometries, attribute limitations, and the absence of dip-line information, which is typically available in 3D seismic datasets.

The FPS attribute integrates similarity, dip variance, dip line polar, fault enhancement filter, energy, and textural entropy, all

385   contributing to an improved classification of faulted regions. Faults near the structural high exhibit stronger FPS values, indicating higher confidence in predictions, whereas polygonal faults in the basinal region show increased misclassification, likely due to their diffuse and discontinuous nature. The stabilization of nRMS and misclassification rates suggests that the model has achieved a balance between learning and generalization, minimizing overfitting while maintaining accurate structural interpretation (Fig. 7).

390   Additionally, the FPS section co-rendered with textural entropy enhances the understanding of fluid migration pathways. In the basin, polygonal faults display high energy values, suggesting shallow fluid migration pathways. However, these faults are capped by fine-grained lithologies dominated by clay, restricting their vertical connectivity to the surface. On either side of

the structural high, there is no evidence of deep-seated fluid migration within the basement rock, indicating that fluid movement is largely confined to the structural high in the ESE and SE sectors. Here, fluid migration appears to be directed towards the

395 surface, where basinal depth decreases and the two structural highs merge into a platform-like configuration. This suggests a preferential migration pathway controlled by fault connectivity and stratigraphic architecture (Figs. 8,9). These faults are observed at strike-line and dip-line directions values ranging between 21,000–23,000 and 9,700–12,000, respectively (Figs. 8-9).

400 **5.3 Attribute extraction and neural computation Pitfalls**

The use of 2D seismic data for attribute extraction and neural computation presents multiple challenges and limitations. The nRMS and misclassification rates, ranging between 0.5 to 0.75 and 20-25%, respectively, were derived from 29 out of 40 seismic sections. However, several seismic sections exhibited significant fluctuations in both training and test nRMS and misclassification rates, indicating that the model has not yet reached complete stability. The continuous adjustment of weights

405 suggests that some models have not fully converged, particularly where test datasets fluctuate more than training datasets, leading to higher uncertainty in unseen data. This instability likely stems from:

a) Limited Attribute Generalisation – Neural networks trained on a restricted set of attributes may struggle to generalise fault patterns, particularly in complex geological settings, accurately, b) Constraints of 2D Seismic Data – Neural network-based fault detection in 2D seismic data lacks dip-line direction information, restricting the model's ability to capture 3D fault

410 continuity, leading to increased misclassification and fluctuating error convergence.

Furthermore, questions may arise regarding the necessity of using attributes and neural networks when dealing with high-resolution 2D seismic data. While manual interpretation can provide reasonable insights, it is inherently time-consuming and labour-intensive, often confined to a limited number of seismic slices due to practical constraints. In contrast, this study incorporates a comprehensive dataset of 40 2D seismic lines, allowing for a more extensive fault mapping approach that

415 enhances structural interpretation. Additionally, manual fault picking is subjective, struggles with fault continuity and subtle fault detection, and is prone to misinterpretation, particularly for small-scale fractures. These limitations emphasize the need for automated, attribute-assisted, and machine-learning approaches to improve accuracy and efficiency.

To address these challenges, this research emphasizes the use of seismic attributes and further advances the approach by computing the meta-attribute FPS. FPS provides a quantitative assessment of fault interpretation that surpasses manual picking

420 by offering a confidence interval for fault presence, density, and distribution, thereby enhancing structural analysis with a data-driven approach.
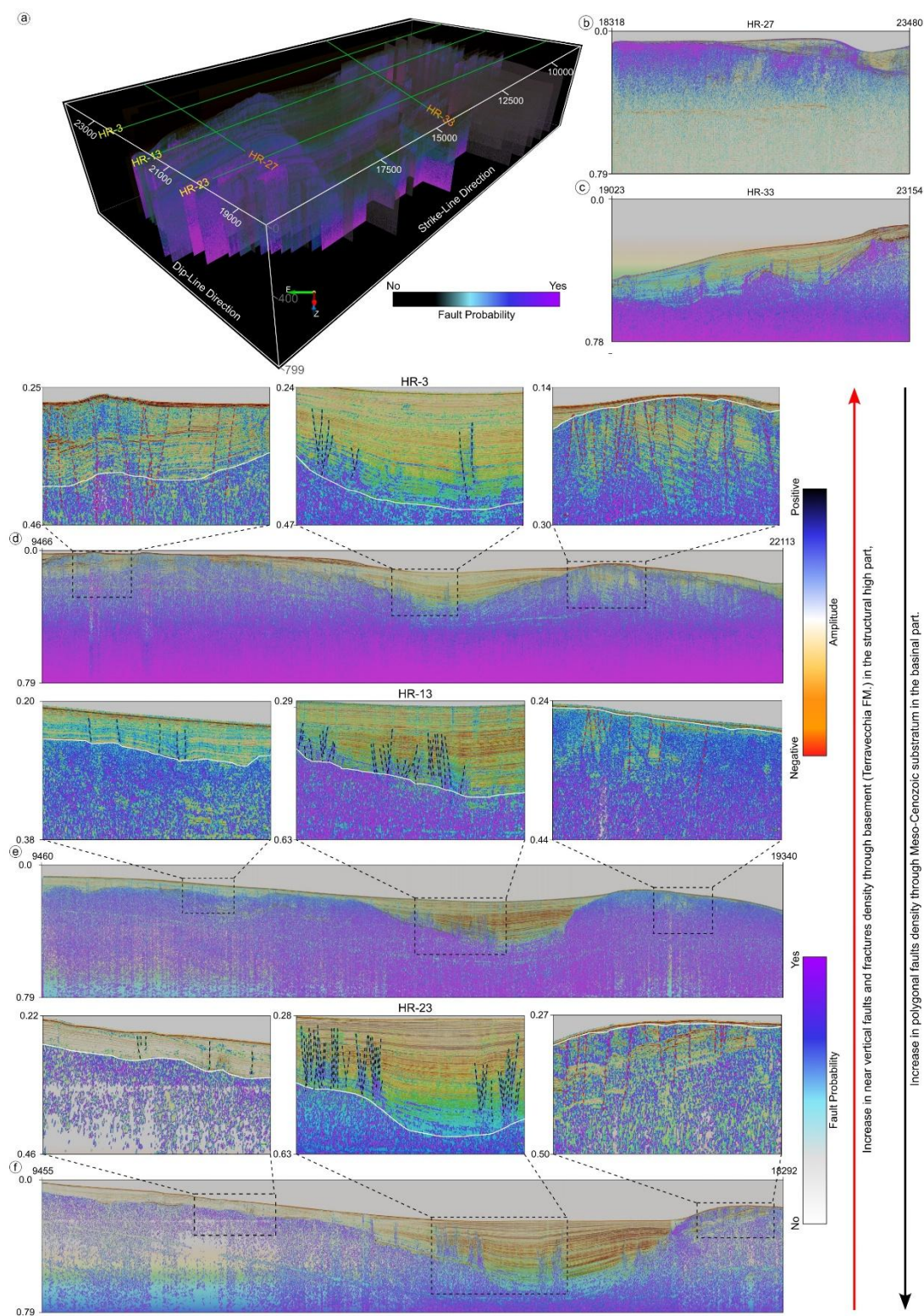
Figure 8: Fault Probability Section (FPS) results applied to 2D seismic sections, integrating machine learning-based fault detection with amplitude data for enhanced fault interpretation. (a) 3D projection of FPS mapped across multiple seismic profiles, showing fault probability variations along in-line and x-line directions. (b–c) Individual seismic sections (HR-27 and HR-33) with FPS overlay, highlighting detected fault networks. (d–h) FPS results for HR-3, HR-7, HR-13, HR-17, and HR-23, demonstrate fault probability variations across different structural settings. The FPS attribute effectively distinguishes high-probability faulted regions near the structural high, while lower probabilities correspond to areas with diffuse or polygonal faulting.

6 Discussion

6.1 Fluid Migration vs Discontinuities

Multiple studies on fluid migration in the Sicily Channel have examined both tectonic and non-tectonic mechanisms, leading to varied fluid escape structures such as pockmarks, gas chimneys, and seepage features. Savini et al. (2009) identified active methane seeps in the Malta Plateau, emphasizing that structural lineaments facilitate fluid migration, aligning with our findings. Micallef et al. (2011) distinguished between tectonic-driven and compaction-induced seepage, demonstrating that polygonal faults contribute to sediment dewatering, while deep-seated faults act as conduits for hydrocarbon migration. Studies by Conte et al. (2014) and Spatola et al. (2018a, 2018b, 2023) explored the role of submarine volcanic activity and morpho-bathymetric changes in fluid seepage. Additionally, Ferrante et al. (2022) and Civile et al. (2023) documented deep and shallow gas accumulations influenced by structural discontinuities.

A recent study by Maiorana et al. (2024)—which directly precedes this research in both study area and thematic focus— proposes two distinct fluid sources:

(i) A deeper gas-rich source (700–820 m b.s.l.) at the Amerillo–Fortuna Formation boundary, confined within sandy lenses of the Terravecchia Fm.

(ii) A shallower oil-bearing source (242–282 m b.s.l.) in the Fortuna Fm., directly linked to pockmark formation.

Fluid migration occurs through (a) dewatering and compaction, forming polygonal faults and gas chimneys, or (b) diffusion through sandy lenses, resulting in dispersed seepage. Furthermore, Maiorana et al. (2024) suggest that pockmarks in the Adventure Plateau are primarily shaped by bottom currents, particularly the Adventure Bank Vortex (ABV).

Building upon previous research, our study introduces a quantitative approach to fault-fluid interactions using seismic attributes and machine learning-based FPS computation. We systematically differentiate fault-controlled vs. non-fault-controlled fluid seepage by analyzing seismic discontinuities. Near-vertical faults near the structural high cross-cut the basement (Terravecchia Fm.) and extend to the seafloor, with fault density decreasing away from the structural high (Table 1; Figs. 8 and 9). Conversely, polygonal fault density increases toward the basin, yet these faults—although producing shallow biogenic gases (CH_4 and CO_2) as noted by Maiorana et al. (2024)—do not contribute to pockmark formation. MBES data (Figs. 2 and 9) show no evidence of polygonal faults forming pockmarks, indicating that these faults primarily trap biogenic

455 gases within Plio-Quaternary deposits, rather than channeling them to the surface. This is further supported by fault and fracture mapping from seismic attribute analysis and neural network-based fault detection (Figs. 8- 10).
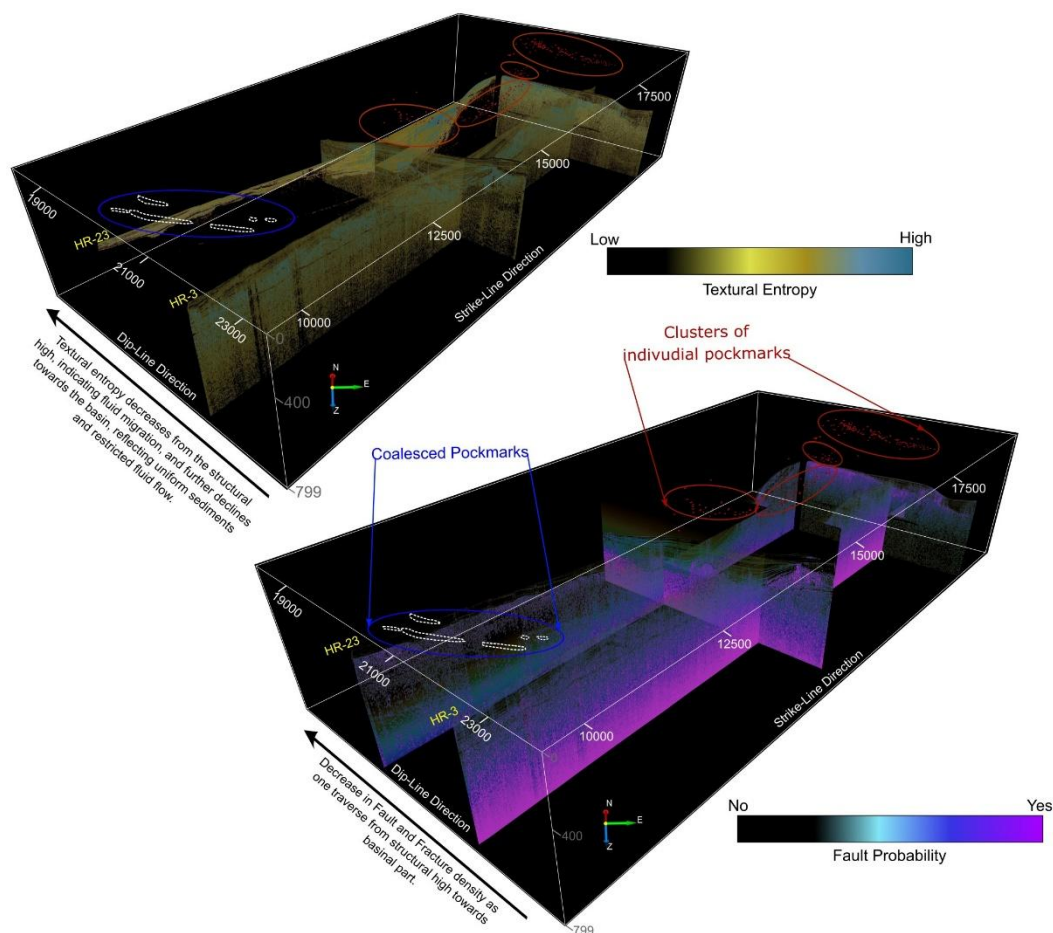
Figure 9: Integrated 3D visualization of fluid migration proxies and fault probability analysis. (Top) Textural entropy highlighting areas of high entropy (black to blue) that correspond to disrupted reflectors and potential fluid pathways. The
460 green ellipses mark the location of individual clusters of pockmarks on the seafloor, which are spatially correlated with areas of high textural entropy. (Bottom) Fault Probability Section visualization, illustrating fault probability distribution across seismic sections. High-probability fault zones (purple to pink) align with pockmark locations.

6.2 Pockmarks: A Proxy for Active Faults

Most earthquakes (approximately 70–80%) are nucleated in oceanic regions, whereas only 20–30% occur in continental
465 settings (Clague, 1997; Jackson, 2001; Wirth et al., 2022). However, this disproportionate occurrence is not reflected in the distribution of studies characterizing seismogenic sources, as most research focuses on continental faults, whether in active fault mapping or paleoseismic event reconstruction (Nakata, 1998; Basili et al., 2008; Malik et al., 2003, 2017; Parrino et al.,

2022, 2023; Srivastava et al., 2023; Malik et al., 2024; Pietrolungo et al., 2024). This skewed distribution is a result of numerous limitations associated with offshore studies, including restricted data availability, limited seismic resolution, difficulty in tracing fault continuity, deep-water imaging constraints, and high operational costs. Additionally, distinguishing tectonic vs. non-tectonic seafloor features is challenging, as fluid escape structures can mimic fault activity, further complicating offshore fault characterization.

Over time, various geophysical techniques have been developed to address these challenges. Dingler et al. (2009) used high-resolution CHIRP seismic data in Lake Tahoe to detect fault offsets, sediment folding, and soft-sediment deformation, providing early evidence of past seismic activity. Nicovich et al. (2024) applied sub-bottom profiling in Henrys Lake, Idaho, to identify liquefaction structures, mass transport deposits, and turbidite layers, aiding in reconstructing earthquake recurrence. Strasser et al. (2024) and Kanamatsu et al. (2023) further refined paleoseismic techniques, using turbidite deposits in deep-sea sediment cores to highlight seismic-triggered sediment remobilization as a key marker of past seismic events. More recently, Leclerc et al. (2024) employed optical imaging to capture high-resolution fault scarp details, while multibeam bathymetry provided broader structural mapping, significantly enhancing offshore fault characterization.

In continuation of these efforts, this research advances the characterization of fault activity by integrating extracted fault and fracture networks with MBES-mapped pockmarks. As previously discussed by Maiorana et al. (2024), two distinct families of pockmarks were identified:

Subcircular pockmarks were interpreted as resulting from vertical fluid escape, likely driven by overpressure and dewatering processes.

Elongated pockmarks were attributed to bottom current activity, particularly the Adventure Bank Vortex (ABV), as their NE-SW orientation does not align with tectonic trends (Fig. 10).

In this manuscript, we further refine this understanding, demonstrating that:

(a) Pockmarks are spatially confined near the structural high, reinforcing a structural control on their distribution.

(b) While ABV currents may reshape pockmarks into elliptical forms, our newly acquired dataset in the SW section reveals that coalesced pockmarks represent relic features, suggesting episodic or past degassing events.

(c) The faults and fractures that cross-cut recent deposits and extend to the seafloor are concentrated near the structural high, with fault density decreasing away from the high, a pattern mirrored in the spatial distribution of pockmarks.

Based on these observations, we propose a hypothesis that the buried NE-SW trending faults in the study area could be active and probably play a key role in guiding pockmark formation on the seafloor (Fig. 10). We further suggest that seafloor morphologies, when analyzed in conjunction with seismic and geophysical datasets, as demonstrated in this study, provide a viable approach for extending active fault studies in offshore regions, overcoming the challenges traditionally associated with deep-water fault characterization.
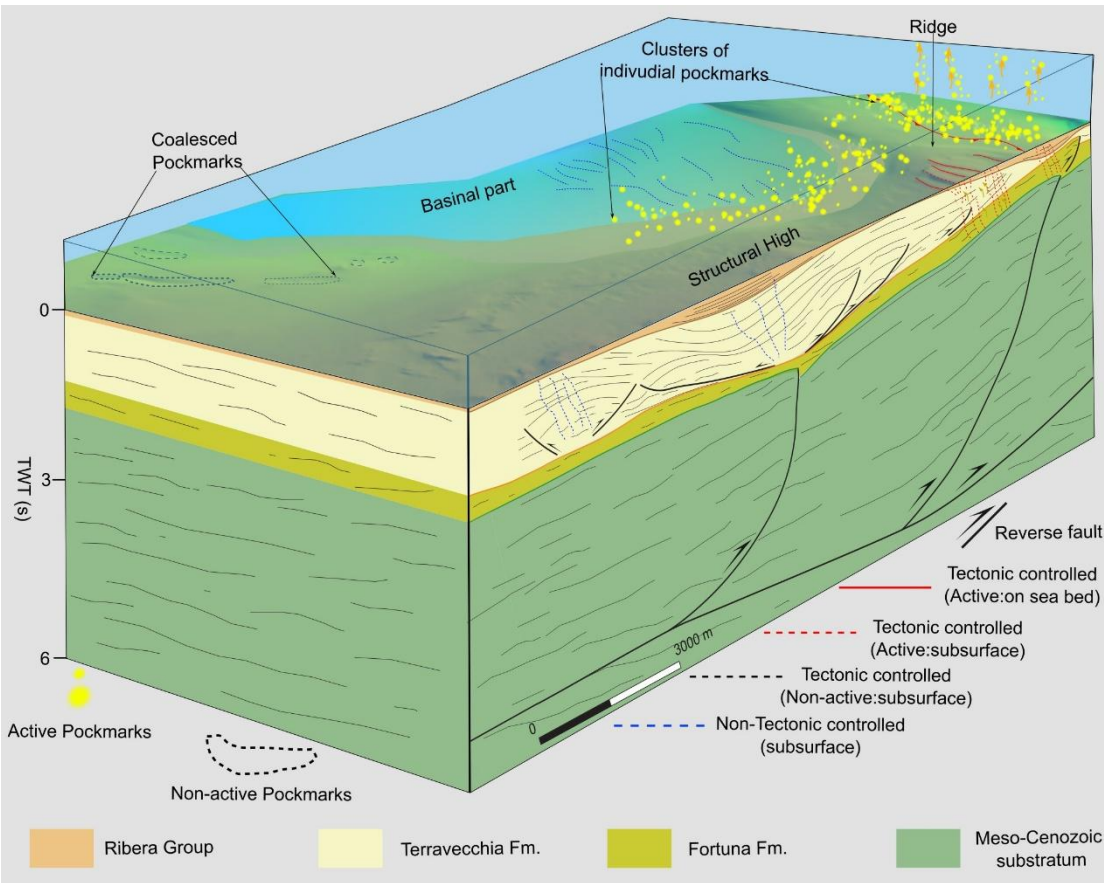
Figure 10: Conceptual model illustrating the relationship between fluid migration, fault activity, and pockmark formation in the study area. The structural high is a key feature influencing fluid pathways, with near-vertical faults acting as conduits for fluid migration from deeper Miocene strata into overlying Plio-Quaternary sequences. The distribution of pockmarks on the seabed is spatially linked to these fault-controlled pathways. Clusters of individual pockmarks (yellow) are primarily located near the structural high, indicating active seepage along fault zones, whereas coalesced pockmarks in the basinal part represent older, inactive seepage features. Faults are categorized based on their tectonic activity: actively migrating fluids to the seabed (solid red), active at subsurface levels (dashed red), and inactive (black). Additionally, non-tectonic subsurface faults (dashed blue) are associated with polygonal faulting within the basin. This model supports the hypothesis that active faults are the primary drivers of fluid escape in the region, with secondary influences from non-tectonic processes such as sediment compaction.

Conclusion

This study presents a different approach to fault activity and fluid migration in the NW Sicily Channel, as it integrates seismic attributes, neural network-based fault detection, and MBES data to refine our understanding of seafloor fluid escape structures and their relationship with active faulting.

Our findings indicate that pockmarks in the study area are spatially correlated with fault networks, particularly near structural highs, where near-vertical faults cross-cut the Terravecchia Formation and extend to the seafloor. Furthermore, our machine-learning-derived Fault Probability Section provides a quantitative measure of fault likelihood, enhancing the accuracy of fault interpretation beyond traditional seismic methods. The absence of significant pockmark formation in polygonal fault-dominated regions, despite the presence of biogenic gas, further supports the idea that tectonic faulting, rather than compaction-driven dewatering alone, governs active fluid migration in the Adventure Plateau.

Based on these observations, we propose that pockmarks serve as proxies for active faulting, providing a novel approach for offshore fault characterization. This method holds significant implications for seismic hazard assessment, hydrocarbon exploration, and geohazard monitoring, especially in regions where traditional fault identification is challenging. Future research should integrate 3D seismic data and geochemical analyses to further validate the role of fault-driven fluid migration in shaping seafloor morphologies.

Data Availability

The multibeam bathymetric data used in this study were acquired using a Teledyne SeaBat T50-P Multibeam Echosounder (MBES) system and processed using CARIS HIPS and SIPS v.10.4. These datasets are not publicly available but can be requested from the respective data providers.

The high-resolution (HR) seismic data analyzed in this study were provided by Copenhagen Offshore Partners (COP), 7 Seas Med srl, and FUGRO. These datasets are proprietary and not publicly accessible. However, one seismic profile used in Figure 2b originates from the ViDEPI public database (https://www.videpi.com/), which provides open-access geophysical data.

Historical earthquake data were obtained from the INGV Seismological Database (https://emidius.mi.ingv.it/CPTI15-DBMI15/query_place/). Seismic attribute analyses and fault probability estimations were performed using OpendTect™ (v7.0.2), for which we gratefully acknowledge dGB Earth Sciences™ for granting an academic license. Machine learning-based fault detection was applied using a Multi-Layer Perceptron (MLP) Neural Network model within the OpendTect™ environment.

Focal mechanism solutions and stress indicators were retrieved from the Global CMT Catalogue (https://www.globalcmt.org/) and the World Stress Map Project (https://www.world-stress-map.org/). Global bathymetric data used for comparison were accessed from the GEBCO 2023 dataset (https://www.gebco.net/).

All processed datasets, seismic attribute calculations, and machine learning models used or generated in this study are available upon request from the corresponding author.

Author Contribution

The conceptualization of the study was done by ES and AS. The seismic data processing, attribute extraction, and machine learning analysis were performed by ES, with methodological support from PCK. Multi-beam data interpretation and geological validation were carried out by ES, FC, MM and AS. The data visualisation and figure preparation were led by ES, with inputs from all co-authors. ES did the writing of the original draft, while review and editing were carried out by FC, MM, PCK and AS. Supervision and project oversight were provided by AS. All authors reviewed and approved the final version of the manuscript.

Competing interests

The authors declare that they have no conflict of interest.

Acknowledgement

We sincerely appreciate Copenhagen Offshore Partners (COP), 7 Seas Med srl, and FUGRO for providing access to the processed seismic dataset. Additionally, we extend our gratitude to dGB Earth Sciences™ for granting an academic license for OpendTect™ (v7.0.2) to the Dipartimento di Scienze della Terra e del Mare (DiSTeM), Università degli Studi di Palermo, Italy.

Financial Support

We acknowledge the CARG Project – Sheet 628 Sciacca (B72C21001150001) to provide financial assistance in carrying out this research.

References

Antonelli, M., Franciosi, R., Pezzi, G., Querci, A., Ronco, G. P., and Vezzani, F.: Paleogeographic evolution and structural setting of the northern side of the Sicily Channel, Memorie della Società Geologica Italiana, 41, 141–157, 1988.

Argnani, A.: The Strait of Sicily rift zone: foreland deformation related to the evolution of a back-arc basin, Journal of Geodynamics, 12, 311–331, 1990.

Basili, R., Valensise, G., Vannoli, P., Burrato, P., Fracassi, U., Mariano, S., Tiberti, M. M., and Boschi, E.: The Database of Individual Seismogenic Sources (DISS), version 3: Summarizing 20 years of research on Italy's earthquake geology, Tectonophysics, 453, 20–43, https://doi.org/10.1016/j.tecto.2007.04.014, 2008.

Basili, R., Danciu, L., Beauval, C., Sesetyan, K., Vilanova, S. P., Adamia, S., Arroucau, P., Atanackov, J., Baize, S., Canora, C., Caputo, R., Carafa, M. M. C., Cushing, E. M., Custódio, S., Demircioglu Tumsa, M. B., Duarte, J. C., Ganas, A., García-

570 Mayordomo, J., Gómez De La Peña, L., Gràcia, E., Jamšek Rupnik, P., Jomard, H., Kastelic, V., Maesano, F. E., Martín-Banda, R., Martínez-Loriente, S., Neres, M., Perea, H., Šket Motnikar, B., Tiberti, M. M., Tsereteli, N., Tsironi, V., Vallone, R., Vanneste, K., Zupančič, P., and Giardini, D.: The European Fault-Source Model 2020 (EFSM20): geologic input data for the European Seismic Hazard Model 2020, Nat. Hazards Earth Syst. Sci., 24, 3945–3976, https://doi.org/10.5194/nhess-24-3945-2024, 2024.

575 Béranger, K., Mortier, L., Gasparini, G.-P., Gervasio, L., Astraldi, M., and Crépon, M.: The dynamics of the Sicily Strait: a comprehensive study from observations and models, Deep Sea Research Part II: Topical Studies in Oceanography, 51, 411–440, 2004.

Bünz, S., Polyanov, S., Vadakkepuliyambatta, S., Consolaro, C., and Mienert, J.: Active gas venting through hydrate-bearing sediments on the Vestnesa Ridge, offshore W-Svalbard, Marine Geology, 332–334, 189–197, https://doi.org/10.1016/j.margeo.2012.09.012, 2012.

580 Catalano, R., Infuso, S., Milia, A., and Sulli, A.: The submerged Sicilian-Maghrebian chain along the Sardinia channel-Sicily straits belt, Geological development of the Sicilian-Tunisian Platform. UNESCO Rep Mar Sci, 58, 43–48, 1993.

Catalano, S., De Guidi, G., Monaco, C., Tortorici, G., and Tortorici, L.: Active faulting and seismicity along the Siculo–Calabrian Rift Zone (southern Italy), Tectonophysics, 453, 177–192, 2008.

Chopra, S. and Marfurt, K.: Curvature attribute applications to 3D surface seismic data, The Leading Edge, 26, 404–414, 585 https://doi.org/10.1190/1.2723201, 2007.

Civile, D., Brancolini, G., Lodolo, E., Forlin, E., Accaino, F., Zecchin, M., and Brancatelli, G.: Morphostructural setting and tectonic evolution of the central part of the Sicilian Channel (central Mediterranean), Lithosphere, 2021, 7866771, 2021.

Civile, D., Baradello, L., Accaino, F., Zecchin, M., Lodolo, E., Ferrante, G. M., Markezic, N., Volpi, V., and Burca, M.: Fluid-Related Features in the Offshore Sector of the Sciacca Geothermal Field (SW Sicily): The Role of the Lithospheric Sciacca 590 Fault System, Geosciences, 13, 231, https://doi.org/10.3390/geosciences13080231, 2023.

Claypool, G. E. and Kaplan, I. R.: The Origin and Distribution of Methane in Marine Sediments, in: Natural Gases in Marine Sediments, edited by: Kaplan, I. R., Springer US, Boston, MA, 99–139, https://doi.org/10.1007/978-1-4684-2757-8_8, 1974.

Dixit, A. and Mandal, A.: Detection of gas chimney and its linkage with deep-seated reservoir in poseidon, NW shelf, Australia from 3D seismic data using multi-attribute analysis and artificial neural network approach, Journal of Natural Gas Science and 595 Engineering, 83, 103586, https://doi.org/10.1016/j.jngse.2020.103586, 2020.

Etiope, G. and Milkov, A. V.: A new estimate of global methane flux from onshore and shallow submarine mud volcanoes to the atmosphere, Env Geol, 46, 997–1002, https://doi.org/10.1007/s00254-004-1085-1, 2004.

Faccenna, C., Piromallo, C., Crespo-Blanc, A., Jolivet, L., and Rossetti, F.: Lateral slab deformation and the origin of the western Mediterranean arcs, Tectonics, 23, 2002TC001488, https://doi.org/10.1029/2002TC001488, 2004.

600 Ferrante, G. M., Accaino, F., Civile, D., Lodolo, E., Volpi, V., Romeo, R., and Accettella, D.: Deep and shallow gas occurrence in the NW Sicilian Channel and related features, Marine and Petroleum Geology, 139, 105575, https://doi.org/10.1016/j.marpetgeo.2022.105575, 2022.

Ferranti, L., Pace, B., Valentini, A., Montagna, P., Pons-Branchu, E., Tisnérat-Laborde, N., and Maschio, L.: Speleoseismological Constraints on Ground Shaking Threshold and Seismogenic Sources in the Pollino Range (Calabria, 605 Southern Italy), JGR Solid Earth, 124, 5192–5216, https://doi.org/10.1029/2018JB017000, 2019.

Gasparo Morticelli, M., Valenti, V., Catalano, R., Sulli, A., Agate, M., Avellone, G., Albanese, C., Basilone, L., and Gugliotta, C.: Deep controls on foreland basin system evolution along the Sicilian fold and thrust belt, Bulletin de la Societé géologique de France, 186, 273–290, 2015.

610 Gauchery, T., Rovere, M., Pellegrini, C., Cattaneo, A., Campiani, E., and Trincardi, F.: Factors controlling margin instability during the plio-quaternary in the Gela Basin (Strait of Sicily, Mediterranean Sea), Marine and Petroleum Geology, 123, 104767, 2021.

Hovland, M.: The Geomorphology and nature of seabed seepage processes, Bathymetry and Its Applications, 79–104, 2012.

Incarbona, A., Di Stefano, E., Patti, B., Pelosi, N., Bonomo, S., Mazzola, S., Sprovieri, R., Tranchida, G., Zgozi, S., and Bonanno, A.: Holocene millennial-scale productivity variations in the Sicily Channel (Mediterranean Sea), Paleoceanography, 615 23, 2007PA001581, https://doi.org/10.1029/2007PA001581, 2008.

Kumar, P. C. and Mandal, A.: Enhancement of fault interpretation using multi-attribute analysis and artificial neural network (ANN) approach: a case study from Taranaki Basin, New Zealand, Exploration Geophysics, 49, 409–424, https://doi.org/10.1071/EG16072, 2018.

Kumar, P. C., Alves, T. M., and Sain, K.: Submarine canyon systems focusing sub-surface fluid in the Canterbury Basin, South 620 Island, New Zealand, Sci Rep, 11, 16990, https://doi.org/10.1038/s41598-021-96574-3, 2021.

Lafuente, J. G., García, A., Mazzola, S., Quintanilla, L., Delgado, J., Cuttita, A., and Patti, B.: Hydrographic phenomena influencing early life stages of the Sicilian Channel anchovy, Fisheries Oceanography, 11, 31–44, https://doi.org/10.1046/j.1365-2419.2002.00186.x, 2002.

Maiorana, M., Artoni, A., Le Breton, E., Sulli, A., Chizzini, N., and Torelli, L.: Is the Sicily Channel a simple Rifting Zone? 625 New evidence from seismic analysis with geodynamic implications, Tectonophysics, 864, 230019, https://doi.org/10.1016/j.tecto.2023.230019, 2023.

Maiorana, M., Spatola, D., Todaro, S., Caldareri, F., Parente, F., Severini, A., and Sulli, A.: Seismo-stratigraphic and morpho-bathymetric analysis revealing recent fluid-rising phenomena on the Adventure Plateau (northwestern Sicily Channel), Mar Geophys Res, 45, 15, https://doi.org/10.1007/s11001-024-09549-0, 2024.

630 Malik, J. N., Nakata, T., Philip, G., and Virdi, N. S.: Preliminary observations from a trench near Chandigarh, NW Himalaya and their bearing on active faulting, CURRENT SCIENCE, 85, 2003.

Malik, J. N., Gadhavi, M. S., Kothyari, G. C., and Satuluri, S.: Paleo-earthquake signatures from the South Wagad Fault (SWF), Wagad Island, Kachchh, Gujarat, western India: A potential seismic hazard, Journal of Structural Geology, 95, 142–159, https://doi.org/10.1016/j.jsg.2016.12.011, 2017.

635 Malik, J. N., Srivastava, E., Gadhavi, M. S., Livio, F., Sharma, N., Arora, S., Parrino, N., Burrato, P., and Sulli, A.: Holocene surface-rupturing paleo-earthquakes along the Kachchh Mainland Fault: shaping the seismic landscape of Kachchh, Western India, Sci Rep, 14, 11612, https://doi.org/10.1038/s41598-024-62086-z, 2024.

Mandal, A. and Srivastava, E.: Enhanced structural interpretation from 3D seismic data using hybrid attributes: New insights into fault visualization and displacement in Cretaceous formations of the Scotian Basin, offshore Nova Scotia, Marine and 640 Petroleum Geology, 89, 464–478, https://doi.org/10.1016/j.marpetgeo.2017.10.013, 2018.

Marfurt, K. J. and Alves, T. M.: Pitfalls and limitations in seismic attribute interpretation of tectonic features, Interpretation, 3, SB5–SB15, https://doi.org/10.1190/INT-2014-0122.1, 2014.

Micallef, A., Berndt, C., and Debono, G.: Fluid flow systems of the Malta Plateau, Central Mediterranean Sea, Marine Geology, 284, 74–85, https://doi.org/10.1016/j.margeo.2011.03.009, 2011.

645 Micallef, A., Spatola, D., Caracausi, A., Italiano, F., Barreca, G., D'Amico, S., Petronio, L., Coren, F., Facchin, L., and Blanos, R.: Active degassing across the Maltese Islands (Mediterranean Sea) and implications for its neotectonics, Marine and Petroleum Geology, 104, 361–374, 2019.

Nakata, T.: First successful paleoseismic trench study on active faults in the Himalaya, EOS, trans., 79, 1998.

Palano, M., Ferranti, L., Monaco, C., Mattia, M., Aloisi, M., Bruno, V., Cannavò, F., and Siligato, G.: GPS velocity and strain 650 fields in Sicily and southern Calabria, Italy: Updated geodetic constraints on tectonic block interaction in the central Mediterranean, J. Geophys. Res., 117, 2012JB009254, https://doi.org/10.1029/2012JB009254, 2012.

Palano, M., Ursino, A., Spampinato, S., Sparacino, F., Polonia, A., and Gasperini, L.: Crustal deformation, active tectonics and seismic potential in the Sicily Channel (Central Mediterranean), along the Nubia–Eurasia plate boundary, Scientific reports, 10, 21238, 2020.

655 Parrino, N., Pepe, F., Burrato, P., Dardanelli, G., Corradino, M., Pipitone, C., Morticelli, M. G., Sulli, A., and Di Maggio, C.: Elusive active faults in a low strain rate region (Sicily, Italy): Hints from a multidisciplinary land-to-sea approach, Tectonophysics, 839, 229520, https://doi.org/10.1016/j.tecto.2022.229520, 2022.

Parrino, N., Burrato, P., Sulli, A., Gasparo Morticelli, M., Agate, M., Srivastava, E., Malik, J. N., and Di Maggio, C.: Plio-Quaternary coastal landscape evolution of north-western Sicily (Italy), Journal of Maps, 19, 2159889, 660 https://doi.org/10.1080/17445647.2022.2159889, 2023.

Pietrolungo, F., Lavecchia, G., Madarieta-Txurruka, A., Sparacino, F., Srivastava, E., Cirillo, D., De Nardis, R., Andrenacci, C., Bello, S., Parrino, N., Sulli, A., and Palano, M.: Comparison of Crustal Stress and Strain Fields in the Himalaya–Tibet Region: Geodynamic Implications, Remote Sensing, 16, 4765, https://doi.org/10.3390/rs16244765, 2024.

Robinson, A. R., Leslie, W. G., Theocharis, A., and Lascaratos, A.: Mediterranean sea circulation, Ocean currents, 1, 2001.

665 Santinelli, C.: DOC in the Mediterranean Sea, in: Biogeochemistry of marine dissolved organic matter, Elsevier, 579–608, 2015.

Savini, A., Malinverno, E., Etiope, G., Tessarolo, C., and Corselli, C.: Shallow seep-related seafloor features along the Malta plateau (Sicily channel – Mediterranean Sea): Morphologies and geo-environmental control of their distribution, Marine and Petroleum Geology, 26, 1831–1848, https://doi.org/10.1016/j.marpetgeo.2009.04.003, 2009.

670 Spatola, D., Micallef, A., Sulli, A., Basilone, L., and Basilone, G.: Evidence of active fluid seepage (AFS) in the southern region of the central Mediterranean Sea, Measurement, 128, 247–253, https://doi.org/10.1016/j.measurement.2018.06.058, 2018a.

Spatola, D., Micallef, A., Sulli, A., Basilone, L., Ferreri, R., Basilone, G., Bonanno, A., Pulizzi, M., and Mangano, S.: The Graham Bank (Sicily Channel, central Mediterranean Sea): Seafloor signatures of volcanic and tectonic controls, 675 Geomorphology, 318, 375–389, https://doi.org/10.1016/j.geomorph.2018.07.006, 2018b.

Spatola, D., Sulli, A., Basilone, L., Casalbore, D., Napoli, S., Basilone, G., and Chiocci, F. L.: Morphology of the submerged Ferdinandea Island, the 'Neverland' of the Sicily Channel (central Mediterranean Sea), Journal of Maps, 19, 2243305, https://doi.org/10.1080/17445647.2023.2243305, 2023.

Srivastava, E., Mandal, A., and Kumar, P. C.: Seismic data conditioning and multiattribute analysis for enhanced structural
680 interpretation: A case study from offshore Nova Scotia, Scotian Basin, in: SEG Technical Program Expanded Abstracts 2017,
SEG Technical Program Expanded Abstracts 2017, Houston, Texas, 2225–2229, https://doi.org/10.1190/segam2017-
17778902.1, 2017.

Srivastava, E., Malik, J. N., Parrino, N., Burrato, P., Sharma, N., Gadhavi, M., Sulli, A., Di Maggio, C., and Morticelli, M. G.:
Extremely fast Holocene coastal landscape evolution in the Kachchh Upland (NW India): Clues from a multidisciplinary
685 review, Journal of Maps, 1–10, https://doi.org/10.1080/17445647.2023.2167617, 2023.

Stanley, D. J., Maldonado, A., and Stuckenrath, R.: Strait of Sicily depositional rates and patterns, and possible reversal of
currents in the late quaternary, Palaeogeography, Palaeoclimatology, Palaeoecology, 18, 279–291,
https://doi.org/10.1016/0031-0182(75)90037-1, 1975.

Sulli, A., Gasparo Morticelli, M., Agate, M., and Zizzo, E.: Active north-vergent thrusting in the northern Sicily continental
690 margin in the frame of the quaternary evolution of the Sicilian collisional system, Tectonophysics, 802, 228717,
https://doi.org/10.1016/j.tecto.2021.228717, 2021.

Sun, X., Yang, J., Zheng, M., and Zhang, X.: Artificial construction of the biocoenosis of deep-sea ecosystem via seeping
methane, Environmental Microbiology, 23, 1186–1198, https://doi.org/10.1111/1462-2920.15347, 2021.

Volpi, V. and al., et: Seabed and shallow morphological setting of the western Sicilian Channel, BGO,
695 https://doi.org/10.4430/bgo00401, 2022.

Whiticar, M. J.: Carbon and hydrogen isotope systematics of bacterial formation and oxidation of methane, Chemical Geology,
161, 291–314, https://doi.org/10.1016/S0009-2541(99)00092-3, 1999.

Whiticar, M. J.: Diagenetic relationships of methanogenesis, nutrients, acoustic turbidity, pockmarks and freshwater seepages
in Eckernförde Bay, Marine Geology, 182, 29–53, https://doi.org/10.1016/S0025-3227(01)00227-4, 2002.

700 Zhang, G., Wang, X., Li, L., Sun, L., Guo, Y., Lu, Y., Li, W., Wang, Z., Qian, J., Yang, T., and Wang, W.: Gas Hydrate
Accumulation Related to Pockmarks and Faults in the Zhongjiannan Basin, South China Sea, Front. Earth Sci., 10, 902469,
https://doi.org/10.3389/feart.2022.902469, 2022.